Gaussian process with physical laws for 3D cardiac modeling

Masahiro Nakano*, Ryohei Shibue*, Kunio Kashino*, Shingo Tsukada*, Hitonobu Tomoike*†
*NTT Basic Research Laboratories, NTT corporation
Atsugi, Kanagawa 243-0198, Japan
{masahiro.nakano.pr, ryohei.shibue.vk, kunio.kashino.me, shingo.tsukada.aw, hitonobu.tomoike.ez}@hco.ntt.co.jp

†Medical and Health Information Laboratories, NTT Incorporated

***Abstract*—This paper introduces some physical laws into a Gaussian process for a statistical three-dimensional (3D) cardiac computational model. The 3D cardiac shape modeling is still challenging, since it involves personality and diversity. However, in spite of such variety, the heart shape must be ruled by some physical laws, which should be an important clue for the statistical shape estimation. Specifically, we introduce the Frank-Starling laws into the Gaussian process as a linear constraint, whose resulting process also follows a Gaussian process. For demonstration, we apply our model into the pipeline that estimates the heart shape from cardiovascular magnetic resonance (CMR) imaging, by combining it with the deep neural networks-based anatomical segmentation of CMR imaging.**

***Index Terms*—Gaussian process, Statistical shape model, Cardiac modeling, Frank-Starling laws**

I. Introduction

Cardiovascular disease is one of the leading causes of both morbidity and mortality all over the world. For example, heart failure is the decline of cardiac function, which leads to insufficient blood delivery to the organs [9], [12]. About 1-2% of the adult population is affected, and the incidence rate among 70 years and older is even above 10% [17]. Early diagnosis and treatment planning are demanded for the wide variety of etiologies and pathophysiologies. As demonstrated in intensive research in the field of computational biology in the last decades, three-dimensional (3D) cardiac computational models have the potential ability to give us a clue to perform early diagnosis or to have high affinity with machine learning for treatment planning. However, 3D cardiac modeling with the personalization and diversity which reflects abnormal behaviors of cardiac function remains challenging.

Multi-modality must be a promising direction of more sophisticated 3D cardiac modeling. Currently, there have been a variety of methods for measuring structure and function of the heart, including cardiac imaging, electrocardiography, and blood pressure [13]. For example, cardiac anatomy and function can be assessed by various imaging modalities such as ultrasound, magnetic resonance, and computed tomography. For another example, electrical activity of the heart can be also obtained indirectly using electrodes on the surface of the body, which detect small electrical gradients caused by the depolarization. Actually, these side information must become clues to cardiac models. However, multi-modal measurements might take a high cost, and sometimes be essentially intractable. For example, in principle, we cannot simultaneously obtain magnetic resonance and heart sounds. Motivated from this, we take the first step towards multi-modal cardiac modeling in an unsupervised manner, and focus on some physical laws which have high affinity with statistical models, such as the Gaussian process.

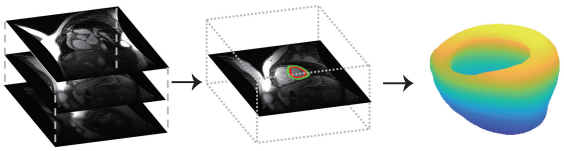

Fig. 1. Illustration of pipeline of cardiac modeling. **Left:** Cardiovascular magnetic resonance (CMR) imaging. **Middle:** Segmentation of CMR imaging. We rely on a state-of-the-art method based on the deep learning network for this phase. **Right:** 3D cardiac modeling as a regression problem, which is our main focus of this paper.

In computer vision and graphics, the Gaussian process (GP) [11], [18] is one of the standard tools to represent statistical models of target objects containing some uncertainty. We can actually employ the usual GP prior to learn surfaces of anatomical regions of the heart. However, the standard use of the GP can typically capture only smoothness of the surfaces, and lacks other features of the heart shape. Therefore, we introduce some physical laws of the heart as linear constraints to the GP. As a result, the learned function from the constrained GP prior is to be ruled by the physical laws.

Our contributions of this paper for 3D cardiac modeling consist of the following two issues:

- We propose a Bayesian nonparametric approach for 3D (4D with time axis) cardiac computational model, which introduces physical laws into the statistical shape model in an unsupervised manner.
- We construct a constrained Gaussian process, whose constraints are described by integral operator.

II. Preliminaries

A. Gaussian process for statistical shape model

A Gaussian process (GP) is the Bayesian nonparametric model, that consists of a collection of random variables,

any finite number of which are jointly Gaussian. The GP is typically used for a prior of a distribution over functions $\mathbb{R}^d$:

$$f(\mathbf{x}) \sim \mathcal{GP}(\mu(\mathbf{x}), k(\mathbf{x}, \mathbf{x}')), \tag{1}$$

where $\mu : \mathbb{R}^d \to \mathbb{R}$ is a mean field, and $k : \mathbb{R}^d \times \mathbb{R}^d \to \mathbb{R}$ is a symmetric and positive semi-definite covariance kernel. As a telling application of the GP, the regression problem can be described as follows: We suppose a nonparametric regression model $y_k = f(\mathbf{x}_k) + e_k$, where e_k is zero-mean white noise representing the measurement uncertainty. Given the input data $(\mathbf{x}_k, y_k)_{k=1}^N$, we would find a posterior over the function $f(\mathbf{x})$. Needless to say, the efficacy of the GP regression problem depends on whether we choose appropriate mean and covariance functions, and appropriately tune their associated hyper-parameters, which are strongly related to prior knowledge of the underlying problem.

Constrained Gaussian process [8] - One might hope another method to refine the GP regression problem. Specifically, we consider how to directly introduce some constraint on f. We suppose that certain constraints are fulfilled by the following equation:

$$\mathfrak{F}_{\mathbf{x}}[f] = 0, \tag{2}$$

where $\mathfrak{F}_{\mathbf{x}}$ is an operator mapping the function $f(\mathbf{x})$ to another function $h(\mathbf{x})$: $\mathfrak{F}_{\mathbf{x}}[f] = h$. Equation (2) may come from prior knowledge of f, depending on applications, physical laws, and tendency of input data. This formulation has the advantage that the GP prior directly obeys the constraint, Equation (2), instead of indirectly tuning mean and covariance functions.

We move on to how to obtain the GP prior such that the function f holds Equation (2). The key is that GPs are closed under linear operators, just as Gaussian distributions are closed under linear transformations [8]. We deal with $f(\mathbf{x})$ to be related to another function $g(\mathbf{x})$ via some operator $\mathfrak{G}_{\mathbf{x}}$:

$$f = \mathfrak{G}_{\mathbf{x}}[g]. \tag{3}$$

As a result, the constraint, Equation (2), follows

$$\mathfrak{F}_{\mathbf{x}}[\mathfrak{G}_{\mathbf{x}}[g]] = 0. \tag{4}$$

Owing to the fact that GPs are closed under linear operators, we have

$$f = \mathfrak{G}_{\mathbf{x}} g \sim \mathcal{GP}(\mathfrak{G}_{\mathbf{x}} \mu_g, \mathfrak{G}_{\mathbf{x}} K_g \mathfrak{G}_{\mathbf{x}'}^{\mathrm{T}}). \tag{5}$$

Consequently, the problem is reduced to how to find suitable operators $\mathfrak{G}_{\mathbf{x}}$ given the constraints corresponding to $\mathfrak{F}_{\mathbf{x}}$. In this paper, we focus on physical laws of the heart for suitable operators $\mathfrak{G}_{\mathbf{x}}$.

B. Physical laws of heart

The Frank-Starling law of the heart provides the relationship between stroke volume and end diastolic volume, which gives us a clue for time-varying volumes of the left/right ventricular for a single cardiac cycle. The cycle can be broadly classified into four stages: ventricular filling derived from mitral valve opening, isovolumetric contraction from mitral valve closing, ejection from aortic valve opening, and isovolumetric relaxation from aortic valve closing. As shown in Figure 2, the volume evolutions are moderate at the 2nd and 4th stages, while they are radical at the 1st and 3rd stages.

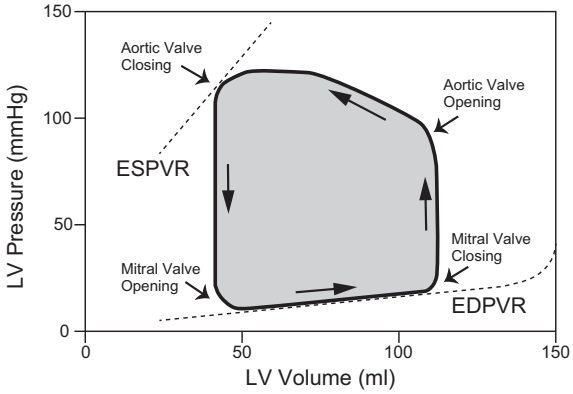

Fig. 2. Illustration of pressure-volume curve. The cycle can be classified into four stages: ventricular filling, isovolumetric contraction, ejection, and isovolumetric. The maximal pressure is bounded as the end-systolic pressure volume relationship (ESPVR). End-diastolic pressure volume relationship describes the passive filling curve for the ventricle. We can interpret the 4 stages of the single cycle as the 4-state hidden Markov model.

C. Preprocessing for cardiac modeling

Our method for cardiac computational modeling consists of two stages. The former one (Figure 1, from left to center) corresponds to automatic segmentation of 3D images of heart obtained from raw cardiac magnetic resonance imaging (MRI) into 5 classes, consisting of the left ventricular cavity (LVC), right ventricular cavity (RVC), left ventricular wall (LVW), right ventricular wall (RVW), and background. For this, we rely on a current state-of-the-art technology based on the multi-task deep learning network. The latter one (Figure 1, from center to right) is our main contribution, which learn a statistical cardiac computational model based on the GP prior from segmentation of cardiac MRI.

Raw data - First of all, we would like to emphasize that the raw data must essentially contain some statistical uncertainty, which should be handled as statistical models. Cardiovascular magnetic resonance (CMR) imaging is the gold standard for assessing cardiac chamber volume and mass for a wide range of cardiovascular diseases. As a matter of practice, two types of CMR volumetric inputs are handled: low-resolution and high-resolution volumes. The low-resolution volume has a large slice thickness, giving rise to a staircase effect in the long-axis view. Additionally, since the slice are usually acquired from multiple breath-holds, inconsistency of each breath-hold results in an inter-slice shift artefact. On the other hand, high-resolution imaging requires only one single 20-25 second breath-hold, which may avoid inter-slice shift artefact. Consequently, motivated from this issue, we believe that statistical models have high affinity with this kind of data.

Segmentation of CMR imaging - This component relies on a state-of-the-art method based on the multi-task deep learning network [23], which predicts segmentation labels with

anatomical clues in CMR volumes. The network takes input volumetric images as multi-channel vector images, requires no region of interest extraction, and contains up to 15 convolutional layers. The network simultaneously capture the segmentation labels and anatomical landmarks in CMR volumes, which has computational advantage of 2D networks and is able to address 3D issues without compromising accuracy and spatial consistency.

III. Cardiac model

We focus on the time evolution of the cardiac surfaces of the LVC or the RVC. We suppose that observations consist of a collection of points on $\mathbb{R}^4$ of the three-dimensional orthogonal coordinates with (discrete) time stamps, which are *candidates* of the cardiac surface but includes some uncertainty indicates. Our hope is to know the function $f_1 : \mathbb{R}^3 \to \mathbb{R}$ such that $z = f_1(x, y, t)$ for any points $(x, y, t) \in \mathbb{R}^3$ on the *true* cardiac surface. In order to make f_1 be injective, we divide the problem into two cases, $z \geq 0$ and $z < 0$. That is, the whole heart is divided into two hemispheres. In the following, we consider the case $z \geq 0$, which is immediately applied to the other case $z < 0$ with slight modification.

The key of our method is to introduce the time evolution of the volume of the LVC (or RVC) into the GP model. We introduce a function $f_2 : \mathbb{R} \to \mathbb{R}$, and suppose that the volume of the LVC (or RVC) at the time t is represented by $f_2(t)$. Then we have

$$\int_D f_1(x, y, t)dxdy - f_2(t) = 0 \quad \text{for any } t, \tag{6}$$

where D is a large region of (x, y) on $\mathbb{R}^2$, and assume $f_1(x, y, t) = 0$ for (x, y, t) which is outside of the hearts.

Our target is to find suitable f_1 and f_2 such that the following additional constraints:

Physical law - As shown in Figure 2, the volume evolution f_2 can be interpreted as a sequence of the transition of hidden 4 states. This implies the following conditions:

Data-driven physical law

State $\#\mathbf{1}$ (from mitral valve opening to mitral valve closing) - The volume almost never change. It is allowed to be self-transition or go to the state $\#2$.
State $\#\mathbf{2}$ (from mitral valve closing to aortic valve opening) - The volume must monotonically increase. It is allowed to be self-transition or go to the state $\#3$.
State $\#\mathbf{3}$ (from aortic valve opening to aortic valve closing) - The volume almost never change. It is allowed to be self-transition or go to the state $\#4$.
State $\#\mathbf{4}$ (from aortic valve closing to mitral valve opening) - The volume must monotonically decrease. It is allowed to be self-transition or go to the state $\#1$.

In summary, the sequence of the differential value of f_2 is the observation of the following HMM:

$$f_2(t+1) - f_2(t) \sim \begin{cases} \mathrm{Normal}(0, \sigma) & (Z_t = 1) \\ \mathrm{Gamma}(\alpha_1, \beta_1) & (Z_t = 2) \\ \mathrm{Normal}(0, \sigma) & (Z_t = 3) \\ -\mathrm{Gamma}(\alpha_2, \beta_2) & (Z_t = 4), \end{cases} \tag{7}$$

where Z_t represents the index of hidden states at tth time. The sequence of the state transition $Z_1, Z_2, \ldots$ can be expressed as $Z_{t+1} \mid Z_t \sim \mathrm{Categorical}(P_{Z_t,1}, P_{Z_t,2}, P_{Z_t,3}, P_{Z_t,4})$, where

$$P = \begin{pmatrix} p_1 & 1-p_1 & 0 & 0 \\ 0 & p_2 & 1-p_2 & 0 \\ 0 & 0 & p_3 & 1-p_3 \\ 1-p_4 & 0 & 0 & p_4 \end{pmatrix}, \tag{8}$$

and p_1, p_2, p_3, p_4 are hyper-parameters drawn from the non-informative beta distribution.

Finally, our model for $f = [f_1, f_2]^{\mathrm{T}}$ can be formulated as the linearly constrained GP. The operator matrix $\mathfrak{F}_{\mathbf{x}}$ corresponding to the constraint, Equation (6), is expressed as

$$\mathfrak{F}_{\mathbf{x}}[f] = \begin{bmatrix} \int_D dxdy & -\mathrm{id}_{\mathbb{R}} \end{bmatrix} \begin{bmatrix} f_1 \\ f_2 \end{bmatrix}, \tag{9}$$

where $\mathrm{id}_{\mathbb{R}}$ denotes the identity map on $\mathbb{R}$. Therefore, we obtain the following operator matrix $\mathfrak{G}_{\mathbf{x}}$:

$$\mathfrak{G}_{\mathbf{x}} = \begin{bmatrix} \mathrm{id}_{\mathbb{R}} \\ \int_D dxdy \end{bmatrix}, \tag{10}$$

such that $\mathfrak{F}_{\mathbf{x}}\mathfrak{G}_{\mathbf{x}} = 0$. Consequently, using $\mathfrak{G}_{\mathbf{x}}$, we obtain the following model for the target function: $f(\mathbf{x}) \sim \mathcal{GP}(\mathfrak{G}_{\mathbf{x}}\mu_g, \mathfrak{G}_{\mathbf{x}}K_g\mathfrak{G}_{\mathbf{x}'}^{\mathrm{T}})$, for any underlying function $g(\mathbf{x}) \sim \mathcal{GP}(\mu_g, K_g)$. For each $g(x, y, t)$, we can employ the GP with no constraints trained in advance.

Bayesian inference method - For space limitations, we omit the detail. However, we can apply usual Bayesian methods into our model. Specifically, we employed the Markov chain Monte Carlo method which repeatedly iterates over the updates of the GP for f and the HMM for derivatives of f_2 until convergence.

IV. Related work

Multi-modality - Recently, there have been 3D cardiac modeling methods from a variety of 3D imaging modalities, including computed tomography, magnetic resonance imaging or ultrasound, whose model parameters are automatically determined from imaging data using a database-guided machine learning (ML) framework [7], [22]. To achieve robust parameter estimation for complex cardiac models, various algorithms have been proposed, including discriminative learning methods with semantic constraints [6], [16]. Our contribution on this line of research is to explicitly employ physical laws in order to more accurately capture the detail shape of the heart in an unsupervised manner.

Relationship to segmentation tasks - Our method relies on automatic segmentation whose state-of-the-art performance has been achieved by deep neural networks [2], [5], [14], [15], [19], [23] as preprocessing for raw cardiac MRI. We here emphasize that 3D cardiac modeling is actually related to

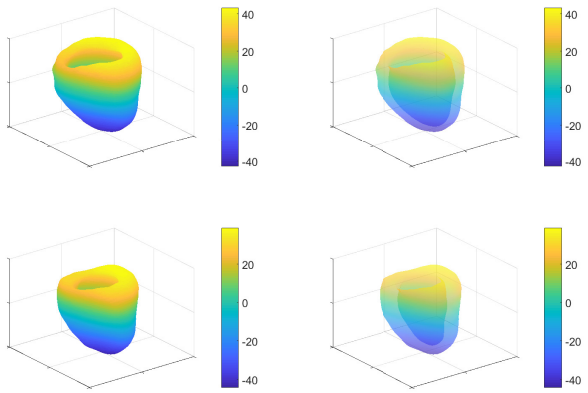

Fig. 3. 3D models of left ventricular. **Top Left:** Epicardium at end-diastolic phase. **Top Right:** Endocardium at end-diastolic phase. **Bottom Left:** Epicardium at end-systolic phase. **Bottom Right:** Endocardium at end-systolic phase. The color map shows the vertical contour.

segmentation task of cardiac imaging, however, they are definitely distinctive issues. Typically, segmentation algorithms mainly focus on classification of each voxel (point) into anatomical labels. On the other hand, 3D cardiac model care about statistical shape model of heart components. Therefore, our method employ automatic segmentation algorithms as preprocessing raw cardiac MRI.

Other shape models - Another popular line of 3D cardiac modeling is the use of the active shape model (ASM) [4] and the morphable model (MM) [3]. Recently, Bayesian nonparametric extension of them using the Gaussian process has been proposed [10], which includes classical ASMs and MMs as special cases. This implies that our strategy (the use of the constrained GP) can be also applicable to this line of research.

V. Experiment

For demonstration, Figure 3 shows 3D models of left ventricular. For evaluation, we employ the York 4D Cardiac MRI dataset [1] (http://www.cse.yorku.ca/ mridataset/), which consists of 33 subjects, each of whose sequence has 20 frames and 8-15 slices, for a total of 7980 images. This dataset also includes the contours corresponding to both the endocardium and epicardium of the left ventricle. Each contour is manually assigned by the first author of [1] as 32 points given in pixel coordinates. We use the endocardium represented by 32 points as a collection of the true points on the endocardium, and calculate the mean squared error (MSE) between the true point and the corresponding point on the estimated surface. For comparison, we employ the GP with no constraint (referred to as GP-base) as a baseline model. We compare the MSE of the GP-FS with that of the GP-base.

Figure 4 shows a MSE comparison between the GP-FS and the GP-base. For 29 subjects out of 33, the GP-FS shows better performance than the GP-base. This means that the FS law constraint for the GP leads to slightly better modifications of the local endocardium surface. Figure 5 shows examples of predictive endocardium obtained from the GP-FS and the GP-base for the first subject of the York 4D Cardiac MRI dataset. We extracted the time-varying endocardium on the 7th slice. While the GP-base is able to essentially capture only smoothness of the surface, the GP-FS handles the global features of the time-varying surface through the HMM derived from the FS law. Therefore, the GP-FS can slightly modify the surface (whose local details have large uncertainty as the GP posterior) according to the FS law.

VI. Conclusion and future work

This paper introduced the Frank-Starling law into the Gaussian process-based 3D statistical cardiac model. We employed the Frank-Starling law as the hidden Markov model of the volume evolution of the endocardium of the left ventricular. We introduced the HMM derived from the Frank-Starling law into the GP as a linear constraint, whose resulting stochastic process again leads to another GP.

In the near future, two promising directions of research are (1) end-to-end learning from the raw cardiac MRI to the 3D or 4D shape model of the heart, and (2) extension to multi-modal models, such as heart sound, electrocardiography, and blood pressure. For the latter one, Classification of Heart Sound Recordings - The PhysioNet Computing in Cardiology Challenge 2016 (https://www.physionet.org/content/challenge-2016/1.0.0/) provided a HMM-based segmentation method [20], [21] of heart sounds as a baseline, which must have high affinity with our GP with the HMM constraint.

References

[1] Alexander Andreopoulos and John K. Tsotsos. Efficient and Generalizable Statistical Models of Shape and Appearance for Analysis of Cardiac MRI. In *Medical Image Analysis*, volume 12, pages 335–357, 2008.

[2] M. Avendi, A. Kheradvar, and H. Jafarkhani. A combined deep-learning and deformable-model approach to fully automatic segmentation of the left ventricle in cardiac MRI. In *Medical Image Analysis*, volume 30, pages 108–119, 2016.

[3] V. Blanz and T. Vetter. A morphable model for the synthesis of 3D faces. In *Proceedings of the 26th annual conference on Computer graphics and interactive techniques*, pages 187–194, 1999.

[4] T. F. Cootes, C. J. Taylor, D. H. Cooper, J. Graham, et al. Active shape models - their training and application. In *Computer Vision and Image Understanding*, volume 61, pages 259–267, 1995.

[5] J. Duan, J. Schlemper, W. Bai, T. J. Dawes, G. Bello, G. Doumou, A. De Marvao, D. P. ORegan, and D. Rueckert. Deep nested level sets: Fully automated segmentation of cardiac MR images in patients with pulmonary hypertension. In *MICCAI*, pages 595–603, 2018.

[6] A. F. Frangi, W. J. Niessen, and M. Viergever. Three-dimensionalModeling for Functional Analysis of Cardiac Images, a Review. In *IEEE Transactions on Medical Imaging*, volume 20, pages 2–5, 2001.

[7] B. Georgescu, X. S. Zhou, D. Comaniciu, , and A. Gupta. Database guided segmentation of anatomical structures with complex appearance. In *IEEE Computer Society Conference on Computer Vision and Pattern Recognition*, pages 429–436, 2005.

[8] Carl Jidling, Niklas Wahlström, Adrian Wills, and Thomas B. Schön. Linearly constrained Gaussian processes. In *Advances in Neural Information Processing Systems*, pages 1215–1224, 2017.

[9] D. Lloyd-Jones, R. J. Adams, T. M. Brown, M. Carnethon, S. Dai, G. De Simone, T. B. Ferguson, K. Furie E. Ford, and C. Gillespie. Heart disease and stroke statistics. In *A Report from the American Heart Association*, volume 121, pages 46–215, 2010.

[10] M. Luthi, T. Gerig, C. Jud, and T. Vetter. Gaussian process morphable models. In *IEEE Transactions on Pattern Analysis and Machine Intelligence*, 2017.

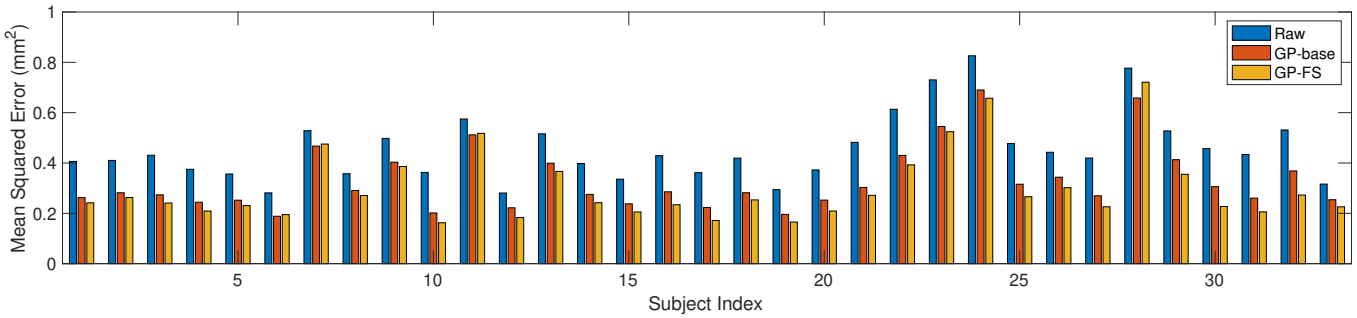

Fig. 4. (Best viewed in color.) MSE comparison between GP-FS and GP-base. For each subject, the left bar shows the MSE of the input data without GP fitting. The center bar and the right bar shows the MSE (between the true point and the corresponding point on the estimated surface) of the GP-base and GP-FS, respectively. For most subjects, the GP-FS shows better performances than the GP-base.

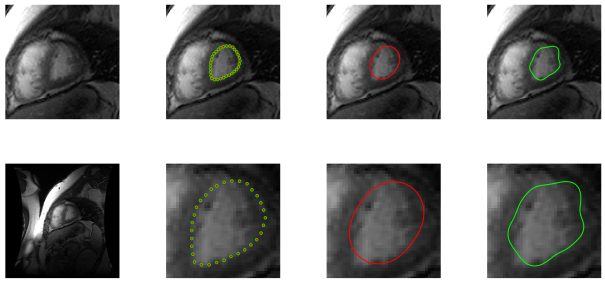

(a) 8th slice on 10th time frame of subject #1.

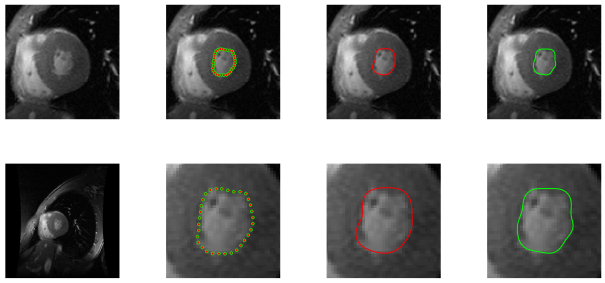

(b) 6th slice on 7th time frame of subject #5.

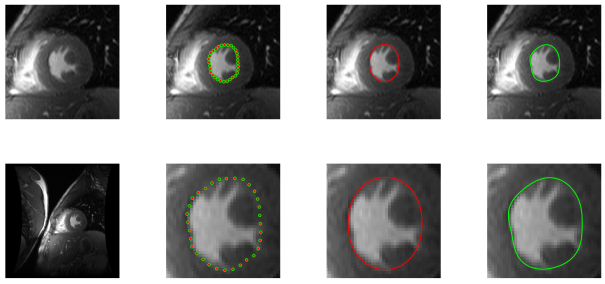

(c) 8th slice on 9th time frame of subject #9.

Fig. 5. (Best viewed in color and zoom-in.) Examples of estimated endocardium from GP-FS and GP-base. From left to right. **First:** Raw MRI (top: focus on endocardium, bottom: raw). **Second:** The true endocardium, described by 32 points manually assigned by the first author of [1] (top: 100-by-100 pixels, bottom: 40-by-40 pixels). **Third:** Predictive endocardium obtained from the GP-base (top: 100-by-100 pixels, bottom: 40-by-40 pixels). **Forth:** Predictive endocardium obtained from the GP-FS (top: 100-by-100 pixels, bottom: 40-by-40 pixels).

[11] M.B.Marcus and Lawrence A. Shepp. Sample behavior of Gaussian processes. In *Proceedings of the sixth Berkeley symposium on mathematical statistics and probability*, volume 2, pages 423–441.

[12] J. McMurray, S. Adamopoulos, S. Anker, A. Auricchio, K. Dickstein, V. Falk, G. Filippatos, C. Fonseca, , and M. Gomez-Sanchez. Esc guidelines for the diagnosis and treatment of acute and chronic heart failure. In *A Report from the American Heart Association*, volume 33, pages 1787–1847, 2012.

[13] Dominik Neumann. *Robust Personalization of Cardiac Computational Models*. PhD thesis, 01 2019.

[14] T. Ngo, Z. Lu, and G. Carneiro. Combining deep learning and level set for the automated segmentation of the left ventricle of the heart from cardiac cine magnetic resonance. In *Medical Image Analysis*, volume 35, pages 159–171.

[15] O. Oktay, E. Ferrante, K. Kamnitsas, M. Heinrich, W. Bai, J. Caballero, S. Cook, A. Marvao, T. Dawes, and D. ORegan. Anatomically Constrained Neural Networks (ACNNs): application to cardiac image enhancement and segmentation. In *IEEE Transaction of Medical Imaging*, volume 37, pages 384–395.

[16] P. Peng, K. Lekadir, A. Gooya, L. Shao, S. E. Petersen, and A. F.Frangi. A Review of Heart Chamber Segmentation for Structural andFunctional Analysis Using Cardiac Magnetic Resonance Imaging. In *Magnetic Resonance Materials in Physics, Biology and Medicine*, volume 29, pages 155–195, 2016.

[17] P. Ponikowski, A. A. Voors, S. D. Anker, H. Bueno, J. G. Cleland, A. J. Coats, V. Falk, J. R. González Juanatey, V.-P. Harjola, and E. A. Jankowska. 2016 ESC Guidelines for the Diagnosis and Treatment of Acuteand Chronic Heart Failure. In *European Heart Journal*, pages 2129–2200, 2016.

[18] Carl Edward Rasmussen and Christopher K. I. Williams. *Gaussian Processes for Machine Learning (Adaptive Computation and Machine Learning)*. The MIT Press, 2005.

[19] J. Schlemper, O. Oktay, W. Bai, D. C. Castro, J. Duan, C. Qin, J. V. Hajnal, and D. Rueckert. Cardiac MR segmentation from undersampled *k*space using deep latent representation learning. In *MICCAI*, pages 259–267.

[20] S. E. Schmidt, C. Holst-Hansen, C. Graff, E. Toft, and J. J. Struijk. Segmentation of heart sound recordings by a duration-dependent hidden Markov model. In *Physiological Measurement*, volume 31, pages 513–529, 2010.

[21] D. B. Springer, L. Tarassenko, and G. D. Clifford. Logistic regression-HSMM-based heart sound segmentation. In *IEEE Transactions on Biomedical Engineering*, pages 513–529, 2015.

[22] Y. Wang, B. Georgescu, T. Chen, W. Wu, P. Wang, X. Lu, R. Ionasec, Y. Zheng, and D. Comaniciu. Learning-based detection and tracking in medical imaging: a probabilistic approach. In *Deformation Models*, pages 209–235, 2013.

[23] Q. Zheng, N. Delingette, Hand Duchateau, and N. Ayache. 3D consistent and robust segmentation of cardiac images by deep learning with spatial propagation. In *IEEE Transaction of Medical Imaging*, 2018.